



Area-to-point regression Kriging approach fusion of Landsat 8 OLI and Sentinel 2 data for assessment of soil macronutrients at Anaimalai, Coimbatore

Dhayalan Vaithyanathan ·
Karuppasamy Sudalaimuthu 

Received: 25 December 2021 / Accepted: 5 April 2022 / Published online: 18 October 2022
© The Author(s), under exclusive licence to Springer Nature Switzerland AG 2022

Abstract Spectral indices-based soil prediction models derived from multispectral datasets are too intricate in terms of accuracy as well as resolution. Complications arise while incorporating multispectral datasets for regional-scale spatial assessment of soil macronutrients. Sporadically satellite image fusion techniques have been used for soil nutrient interpolation to circumvent the complications. The fusion of multispectral bands encompasses precise soil information that cannot be observed as accurate with single satellite dataset. In this study, fusion of near infrared regions of Landsat 8 Operational Land Imager and Sentinel 2 has been observed for its contribution on soil macronutrient assessments. Area-to-point regression Kriging (ATPRK) approach is followed in fusing the two satellite imagery and in situ soil spectral have used for the validation of the resultant. Comparative statistical analysis on Landsat 8 OLI band 5 (wavelength: 845–885 nm), Sentine-2 band 8,8A (wavelength: 785–900 nm) datasets and fused satellite bands provides R^2 values of 0.8209, 0.8436, and 0.8763 respectively. Regression models $y = (0.25006 \pm 0.00754) + (0.0000313)x$, $y = (0.25252 \pm 0.0062) + (0.000810)x$, and $y = (0.23715 \pm 0.0062) + (0.0001210)x$ for nitrogen, phosphorus, and potassium respectively aids

for soil macronutrient interpolation and assessments. Computations reveals the ranges of nitrogen, phosphorus and potassium that floats from 48 to 295 kg/ha, 5.0 to 37 kg/ha, and 32 to 455 kg/ha in the study area. Fusion of satellite imagery by ATPRK approaches in soil macronutrient study at regional scale brings the novelty of the study.

Keywords Multispectral · Landsat 8 OLI · Sentine-2 · Satellite image fusion · Soil macronutrient study

Introduction

Satellite datasets of various resolutions and time series were utilized for precise interpolation and analysis for numerous applications (Rathore et al., 2008). Landsat data owing for its free availability and periodical revisit features with its applications have been globally utilized for various environmental monitoring (Papenfus et al., 2020). History of Landsat data reveals that the Landsat 5 satellite armed with Thematic Mapper (TM) finds major concern in sorting environmental issues and kept monitoring until November 2011; as the descendant of Landsat 5, Landsat 7 evolved to take the monitoring role of the global issues (Brede et al., 2020). Reverberation of the failure of scan line corrector sensor of Landsat 7 results in furnishing of the dataset with almost 22% dead pixel. With the further existence of Landsat dataset resolving the scan line corrector issue, the

D. Vaithyanathan · K. Sudalaimuthu (✉)
Department of Civil Engineering, SRM Institute of Science and Technology, Kattankulathur, India
e-mail: karuppas@srmist.edu.in

D. Vaithyanathan
e-mail: dv1075@srmist.edu.in

Landsat 7 equipped with Enhanced Thematic Mapper (ETM+) along with Operational Land Imagery (OLI) sensor and Thermal Infrared Sensor (TIS) has been evolved as new generation Landsat 8 OLI imagery (Xu et al., 2021). The two sensors furnish seasonal worldwide coverage at the spatial resolution of 30 m for visible, Near Infrared (NIR) and Short Wave Infrared (SWIR), whereas 100 m spatial resolution for thermal and 15 m for panchromatic. Capability of collecting 725 scenes per day holding the scene size of 185-km-cross-track-by-180-km-along-track intensifies the spectral information. The revisit period is stuck to 16 days that are found to be a hindrance for global temporal monitoring of soil information and most of the cases the acquired Landsat 8 dataset gets contaminated by cloud and other atmospheric hindrance (Prada et al., 2020). Hence, getting cloud and shadow-free imagery atleast once in a month is a great challenging one. Therefore, this particular dataset become unsuitable for temporal monitoring of soil properties in regional scale. For full-fledge utilization of Landsat 8, spectral information spatio-temporal fusion methods need to be incorporated (Shen et al., 2016). Concerning the fusion technology, it is mandatory to study the satellite imagery to be fused with Landsat 8 OLI datasets. Considering the projections and downscaling factors involved in fusion techniques, Sentinel 2 dataset has been accounted as satellite image to be fused with the Landsat 8 OLI dataset (Zhang et al., 2021). Sentinel 2 having similar wavelength and free availability comparing to Landsat 8 OLI datasets finds an alternates to the disadvantages faced by the Landsat such as revisit period and cloud contamination (Wang et al., 2021). Sentinel 2 revisits at every 5 day at a particular region of interest with 10-m spatial resolution. Owing broad swath of 290 km as well as magnificent spatial resolution of up to 10 m, Sentinel 2 dataset enhanced the Satellite Pour l'Observation de la Terre (SPOT) and Landsat. Being multispectral imagery, Sentinel 2 produces thirteen bands among which bands 2, 3, 4, and 8 produce the spectra at 10 m, bands 5, 6, 7, 8a, 11, and 12 produce at 20 m, and bands 1, 9, and 10 produces at 60 m of spatial resolutions. Enhanced revisit time of 10 days with one satellite and 5 days with two satellites provided constant viewing angle and Sentinel 2 data finds great utilities in furnishing high temporal spatial information for real world applications. The bands of Landsat 8 OLI and Sentinel 2 correspond to each other. All the Sentinel 2 and Landsat 8 dataset products are in

identical geographic coordinate system (Bolton et al., 2020). In addition, both the products are assessable at free of cost. These criteria tends to utilize the both the products for sustainable monitoring of world issues. With the numerous available fusion techniques, it made easier to utilize complete positive aspects of both the data products. Although the Sentinel 2 data produce the spectra at fine spatial resolution of 10 m and 20 m when compared to Landsat (30 m), the fusion data imparts the fine information under cloud-free conditions, multiple observations of region of interest, enhanced temporal resolution, and precise spectral information (Wang et al., 2017). In addition, if Sentinel 2 dataset possesses any missing spectral information, any region of interest can be enhanced with the Landsat 8 spectral information and vice-versa (Scheffler et al., 2020). In this study, for the first time, the outcomes of fused Landsat 8 and Sentinel 2 data were utilized for the assessment of soil macronutrients more specifically soil nitrogen, phosphorous, and potassium (NPK). From the extensive literature and various researches, it is revealed that the soil exhibits its inherent spectral behavior at Near Infrared Region (NIR: 780 to 1400 nm) and Short-Wave Infrared (SWIR: 1400 to 3000 nm) (Guimarães et al., 2021). Out of 9 bands of Landsat 8 OLI, three bands (5, 6, and 7) fall at the NIR and SWIR regions; whereas, in the case of Sentinel 2 data, five bands (8, 8a, 9, 10, 11, and 12) out of 12 bands bear the regions of NIR and SWIR (Adiri et al., 2020). R^2 comparison for fused reflectance, Landsat 8 OLI, and Sentinel 2 MSI datasets with the in situ soil spectral reflectance was revealed in this study. For the measurement of in situ soil spectra, having the spectral range of 325 to 1075 nm, FieldSpec® Hand-Held 2TM Spectroradiometer was used. Considering the fact of soil spectral behavior at NIR and SWIR, the wavelength range between 780 and 1075 nm was considered in the study corresponding the band 5 of Landsat 8 OLI, and bands 8 and 8a of Sentinel 2 were taken into account for analysis. Precise assessment of soil macronutrients study introduces the equation developed through linear regression analysis by setting out fused satellite data reflectance and field soil NPK analysis results. The model equation outcome of linear regression analysis rendered as the input for assessment of soil macronutrients for the region of interest and by rendering reclassification of fused Landsat 8 OLI and Sentinel 2 MSI datasets in ArcGIS 10.2 software the reflectance values along with its corresponding NPK level made as input to interpolate the soil macronutrients for each

pixels for the area of interest. The outcome of the study reveals the significance of image fusion technique for assessment of soil macronutrients. Proposed image fusion technique called ATPRK (area-to-point regression Kriging) finds fine outcomes among the various geostatistical approaches such as intensity hue saturation, wavelet transformation, Brovey method of image fusion, PCA (principal component analysis) smoothing filter-based intensity modulation, sparse representation, and high pass filter (Liu & Wang, 2020). Alluring characteristics of ATPRK technique that preserves the spectral information more precisely takes coarse band as variable where the spatial resolution as covariate (Zhou et al., 2021). Downscaling approaches were carried out to match the spatial resolution of fusing satellite images so as to gather fine information from the fused product. Exhibiting a user-friendly approach, ATPRK explicitly takes the size of the pixels, spatial resolution, and point spread function of the sensor into account during fusion which tends to preserve and enhance the spatial resolution and spectral information (Priem et al., 2021). Influenced by the advantageous execution of ATPRK approach in fusion, this research paper indulged the fusion of Landsat 8 OLI and Sentinel 2 MSI dataset for assessment of soil macronutrients. Soil macronutrients, an essential component for plant development, energy metabolism and protein synthesis need continuous and precise monitoring. The aforementioned technique in remote sensing finds applications in assessing soil macronutrients. Local farmers get benefited because of continuous and precise monitoring of soil health. Pixel by pixel assessments of soil health provide formulated information such as multicropping pattern, fertilizer needs, and irrigation schema for agriculturist and policy makers. Soil assessment through fused reflectance through ATPRK technique fulfills the research gaps which were unrevealed so far.

Materials and methods

Area-to-point regression Kriging

Regression-based model (mean of spatial process which are spatially varying) and area-to-point Kriging residual-based downscaling (the variations that remains after the spatial variation i.e. “trend”) are the two steps involved in ATPRK (Armannsson et al., 2021). Let’s consider $A^1_V(X_i)$ as a random vector for pixel V in center to X_i , where

i ranges from 1 to N where N is considered as number of pixels in the coarse band l where l ranges from 1 to L (L denotes the number of coarse band and $A^k_V(X_j)$ as a random vector for pixel C in center to X_j , where j ranges from 1 to NS^2 (S denotes the spatial resolution) in the bands k ($k=1$ to K , where K is the number of bands). $A^1_V(X_i)$ as the primary variable at coarse spatial resolution and $A^k_V(X_j)$ as covariate at fine spatial resolution were fed as inputs outcome variable $A^1_V(X)$ is interpolated for each pixels in all the coarse bands. Regression predictions and the parts of ATPRK were denoted as $A^{\wedge 1}_{V1}(X)$ and $A^{\wedge 1}_{V2}(X)$, the ATPRK interpolation is expressed as

$$A^{\wedge 1}_V(X) = A^{\wedge 1}_{V1}(X) + A^{\wedge 1}_{V2}(X) \tag{1}$$

Considering in band k at the determined location X_0 the interpolated $A^1_V(X_0)$ is in linear transformation of the pixel in the corresponding band k ,

$$A^1_V(X_0) = C_1 A^k_{V1}(X_0) + D_1 \tag{2}$$

Equation (2) found invariant to the spatial scale, C_1 and D_1 are the coefficients in Eq. (2) which are estimated in corresponding to the relationship among recognized coarse band l and up scaled band (A^k_V) form the original band k .

$$A^1_V(X) = C_1 A^k_{V1}(X) + D_1 + R^1_V(X) \tag{3}$$

The C_1 and D_1 coefficients are calculated using least square method. The residual ($R^1_V(X)$) needs to be downscaled to finer spatial resolution where ATPRK renders nest step in order to down scale the coarse residual $R^1_V(X)$ in Eq. (3) to the outcome spatial resolution. The residual at the location X_0 is assessed by

$$A^{\wedge 1}_{V2}(X_0) = \sum_{i=1}^N \lambda_i R^1_V(X_i), \text{ s.t. } \sum_{i=1}^N \lambda_i = 1 \tag{4}$$

where the weight of the i th residual of coarse which is centered at X_i is represented as λ_i and N denotes the number of neighboring pixel of the coarse band. Then the weights are estimated based on the Kriging matrix

$$\begin{pmatrix} \gamma_{l_{VV}}(X_1, X_1) & \cdots & \gamma_{l_{VV}}(X_1, X_N) & 1 \\ \vdots & \ddots & \vdots & \vdots \\ \gamma_{l_{VV}}(X_N, X_1) & \cdots & \gamma_{l_{VV}}(X_N, X_N) & 1 \\ 1 & \cdots & 1 & 0 \end{pmatrix} \times \begin{pmatrix} \lambda_1 \\ \vdots \\ \lambda_N \\ \theta \end{pmatrix} = \begin{pmatrix} \gamma_{l_{VV}}(X_0, X_1) \\ \vdots \\ \gamma_{l_{VV}}(X_0, X_N) \\ 1 \end{pmatrix} \tag{5}$$

For x_i and x_j , their corresponding center pixels in l band having the coarse to coarse semivariogram are

denoted by $\gamma_{VV}^1(x_i, x_j)$; for x_0 and x_j , their corresponding center pixels in 1 band having the fine to coarse semivariogram is denoted by $\gamma_{VV}^1(x_0, x_j)$. θ in matrix (5) denotes Lagrange multiplier. If Euclidean distance among the centroids of two pixel is taken as G and $M_V^1(G)$ is sensor's point spread function, then $\gamma_{VV}^1(G)$ and $\gamma_{VV}^1(G)$ are estimated through convolution of fine to fine semivariogram ($\gamma_{VV}^1(G)$) with the sensor's point spread function ($M_V^1(G)$)

$$\gamma_{VV}^1(G) = \gamma_{VV}^1(G) * M_V^1(G) \quad (6)$$

$$\gamma_{VV}^1(G) = \gamma_{VV}^1(G) * M_V^1(G) * M_V^1(-G) \quad (7)$$

In Eqs. (6) and (7), * represent convolution operator. From the deconvolution of coarse semivariogram, the $\gamma_{VV}^1(G)$ can be estimated by utilizing the coarse residual ($R_V^1(X)$).

Study site and datasets

The study area of the proposed fusion study is done at Anaimalai-Pollachi from Tamilnadu, which lies between 10.662°N and 77.00650°E, located 40 km to the south of Coimbatore district of Tamilnadu, India, has an agricultural land of 20,536 Hectares and been supported by Paramikulam Aliyar Project (PAP). Landsat 8 OLI scene carrying object identifier number LC08_L1T_P_144053_20210318_20210328_02_T1 that covers the Anaimalai block was obtained from U.S. Geological Survey (<https://doi.org/10.5066/P975CC9B>) which possess 11 bands and the acquisition date is 18 March 2021 with UTM/WGS Projection and Path/Row of the scene is 144/33. Sentinel 2 scene carrying the object identifier number S2A_MSIL2A_20210212T050931_N0214_R019_T43 covering the same region of interest was obtained from European Space Agency (<https://scihub.copernicus.eu/dhus/#/home>) having 12 bands and the scene has been captured on 12 February 2021. Both the datasets are having the same projection system and found similarity in the wavelength represented in Fig. 1. The band wavelength of Landsat 8 OLI and Sentinel 2 MSI data is given in Table 1. In this study, band 5 of Landsat 8 OLI and bands 8 and 8a of Sentinel 2 MSI have been considered for the soil assessment since the characteristics of soil predominately inferred in NIR and SWIR regions. Band 5 of Landsat 8 OLI having the spatial resolution of 30 m possesses the multiple reflectance of 0.00002 and additive reflectance of -0.1. The

wavelength of band 5 ranges from 845 to 885 nm that falls in NIR region. Band 8 of Sentinel 2 MSI having 10-m spatial resolution ranges from 785 to 899 nm in wavelength where Band 8A possesses 20-m spatial resolution and wavelength ranges from 855 to 875 nm (NIR Narrow). These two bands were used for fusion study for assessing the soil macronutrients.

Image preprocessing

Two major corrections needed to be rectified for satellite products are atmospheric and radiometric corrections (Moravec et al., 2021). Atmospheric corrections remove the absorption effects and the scattering effects from the surface properties whereas the DN (Digital Number) inaccuracy in the satellite data was rectified by radiometric corrections (Kaman & Makandar, 2021). This may occur due to azimuth and elevation of sun or air conditions. Thus, rectifying the radiometric errors give rise to ground truth irradiance or reflectance (Taddia et al., 2020). In this study, Band 5 of Landsat 8 OLI undergone atmospheric and radiometric corrections in ENVI software utilizing FLASH algorithm. Band 8 and Band 8A of Sentinel 2 were preprocessed using Sen2Cor algorithm in SNAP software to remove the atmospheric and radiometric errors (Shrestha et al., 2021). The datasets are subjected to conversion of DN to reflectance values in ArcGIS software using the coefficient of radiometric rescaling and sun angle provided in the metafile of satellite data product. DN to reflectance values for the study area was obtained as represented in Fig. 2 from the following Eq. (8) (Zheng et al., 2020).

$$L_\lambda = M_L Q_{cal} + A_L \quad (8)$$

where,

L_λ = TOA (Top of Atmosphere) spectral radiance (watts/ (m²* srad* μm)).

M_L = Band-specific multiplicative rescaling factor from the metadata (RADIANCE_MULT_BAND_X, where X is the band number, in our study our band numbers are 5 and 8 for Landsat and Sentinel respectively)

A_L = Band-specific additive rescaling factor from the metadata (RADIANCE_ADD_BAND_X)

Q_{cal} = Quantized and calibrated standard product pixel values (DN)

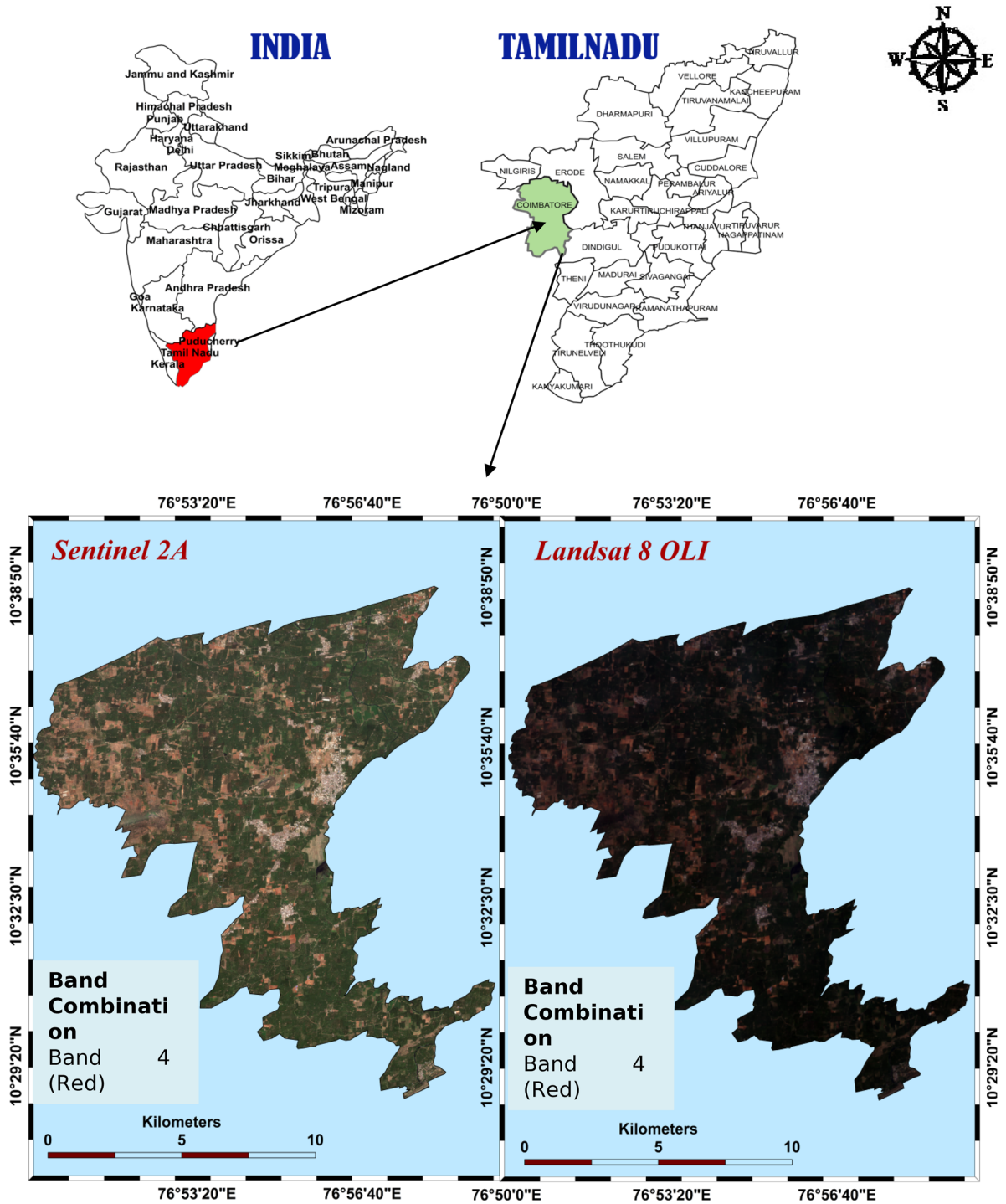


Fig. 1 Sentinel 2 MSI and Landsat 8 OLI of Anaimalai block

Table 1 Band wavelength of Sentinel 2 MSI and Landsat 8 OLI

| Sentinel 2A MSI | | | | Landsat 8 OLI | | | |
|-----------------|-----------------|-----------------------|----------------|---------------|-----------------|-----------------------|----------------|
| Band | Spectral region | Wavelength range (nm) | Resolution (m) | Band | Spectral region | Wavelength range (nm) | Resolution (m) |
| B1 | Coastal aerosol | 433–453 | 60 | B1 | Coastal aerosol | 433–453 | 30 |
| B2 | Blue | 458–523 | 10 | B2 | Blue | 450–515 | 30 |
| B3 | Green Peak | 543–578 | 10 | B3 | Green | 525–600 | 30 |
| B4 | Red | 650–680 | 10 | B4 | Red | 630–680 | 30 |
| B5 | Red Edge 1 | 698–713 | 20 | B5 | NIR | 845–885 | 30 |
| B6 | Red Edge 2 | 733–748 | 20 | B6 | SWIR 1 | 1560–1660 | 30 |
| B7 | Red Edge 3 | 773–793 | 20 | B7 | SWIR 2 | 2100–2300 | 30 |
| B8 | NIR | 785–900 | 10 | B8 | Panchromatic | 500–680 | 15 |
| B8A | NIR Narrow | 855–875 | 20 | B9 | Cirrus | 1360–1390 | 30 |
| B9 | Water Vapor | 935–955 | 60 | B10 | TIRS 1 | 10,600–11,190 | 100–(30) |
| B10 | SWIR/Cirrus | 1360–1390 | 60 | B11 | TIRS 2 | 11,500–12,510 | 100–(30) |
| B11 | SWIR 1 | 1565–1655 | 20 | | | | |
| B12 | SWIR 2 | 2100–2280 | 20 | | | | |

B band, *NIR* near infrared region, *SWIR* short-wave infrared region, *TIRS* thermal infrared region

ATPRK in Landsat 8 OLI and Sentinel 2 MSI

Theoretical concept of ATPRK is implemented for fusion of Landsat 8 OLI and Sentinel 2 MSI dataset. In this study, based on ATPRK approach, 20-m Band 8a of Sentinel 2 is downscaled to 10 m by using 10-m Sentinel 2 band 8 as covariates ($A^k_v(X)$) and the resultant product is termed as ATPRK 1 (Fig. 3a). The 30 m Landsat 8 band 5 is downscaled to 10 m

by using 10-m Sentinel 2 band 8 as covariates and the resultant product is coined as ATPRK 2 (Fig. 3b). This has been done to match the spatial resolution of both the satellite products. This approach meets the requirement of defined criteria such as wavelength, geometry, and the resolution. Here, the 10 m of Band 8 Sentinel 2 MSI data is layer stacked (Fig. 3c) with downscaled Band 8A to make convenient for image fusion. Now the layer-stacked 10-m band 8 of Sentinel

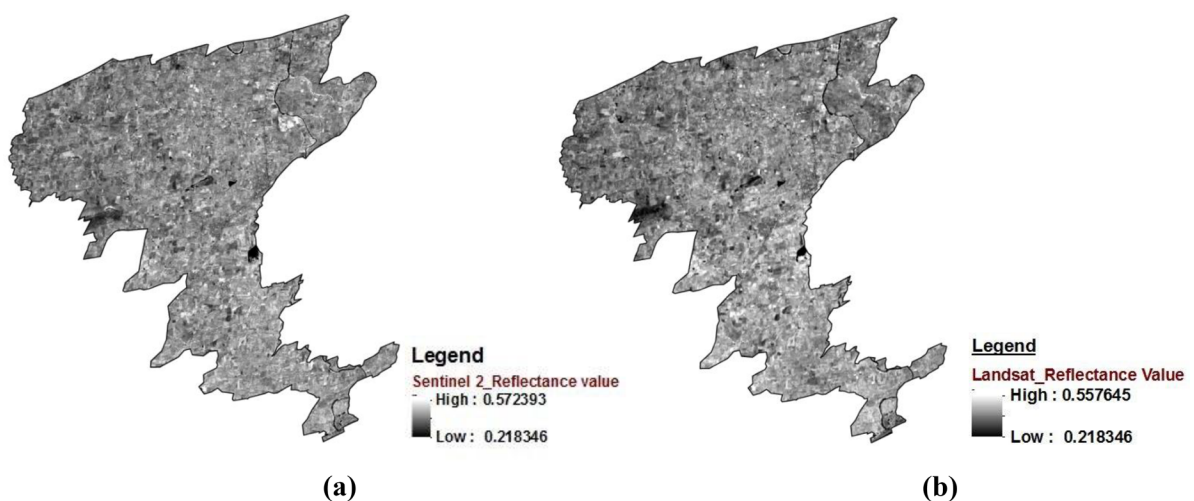


Fig. 2 DN to reflectance of **a** Sentinel 2 MSI (Band 8), **b** Landsat 8 OLI (Band 5)

2A renders numerous spectral information at NIR regions, while the information in Landsat 8 OLI can be retrieved by fusion technique. The spectral missing data in the pixels of Sentinel 2 dataset can be adjusted with the spectral information provided in Landsat 8 OLI data (Chaves et al., 2020). Now the layer-stacked Sentinel 2 10-m data (Band 8A and Band 8) is fused with downscaled 10-m Landsat 8 OLI Band 5 product to produce new data product (Fig. 4) consisting of strong spectral information.

Sampling points and reflectance extraction

Considering the soil characteristics and agricultural practices, about 106 soil samples were collected as represented in Fig. 5 and corresponding GCP (Ground Control Points) of the location is noted with the help of Differential Global Positioning System (DGPS) along with a sub meter (Trimble Navigation Ltd., Sunnyvale, California, USA). The total land parcels were divided into divergent analogous units based on the grids mapped on the region of study. At the depth of 15 cm, the auger were pierced and the soil samples were drawn (Fig. 6a). A total of 15 samples were collected at each nodal point location and mixed as single sample for each location. In the process of mixing the samples the foreign objects were sieved by using 2 mm sieve. Total soil sample collected at per location is reduced by compartmentalization method (Gujre et al., 2021). The soil samples

were air dried to remove the moisture content and packed with labeling (Fig. 6b). Soil samples were subjected to laboratory physio chemical analysis and in situ spectral collection. The basic physical parameters that includes soil pH and electrical conductivity (EC) were computed by a pH meter (Elico LI 617) (Jagadala & Sahoo, 2020) and conductivity meter (Elico CM 183) (Leno et al., 2021) respectively. Soil available nitrogen was analyzed by Kjeldahl method (Dar et al., 2021). Bray-1 method was used to analyze the total phosphorus in the acidic soil whereas Olsen method is used for alkaline soil for estimating soil phosphorus level (Elbasiouny et al., 2020). A flame photometer (Jenway PFP7) (Wiyantoko et al., 2021) was utilized for the fine estimation of available potassium in the soil. Soil health analysis reveals the nitrogen level floats between 44 and 295 kg/Hectare, where the phosphorus ranges from 4.0 to 37.0 kg/Hectare and the potassium ranges from 32 to 455 kg/Hectare. Parallel to soil analysis, in situ soil spectral observation was carried out by using ASD Field-Spec® HandHeld™ 2 spectroradiometer capable of sensing the soil characteristics at the range from 325 to 1075 nm (Jewan et al., 2021). The soil spectra were extracted in the closed laboratory to avoid signal-to-noise errors. The instrument is mounted on the tripod stand and artificial light source is made with the help of tungsten quartz halogen lamp. The soil sample placed at the distance of 30 cm from the instrument. After initial calibration and optimization

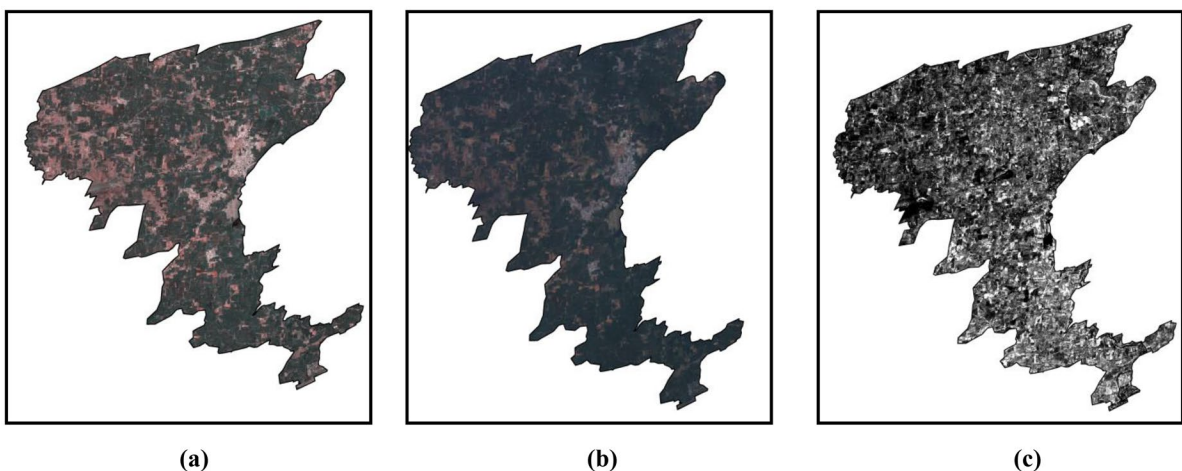
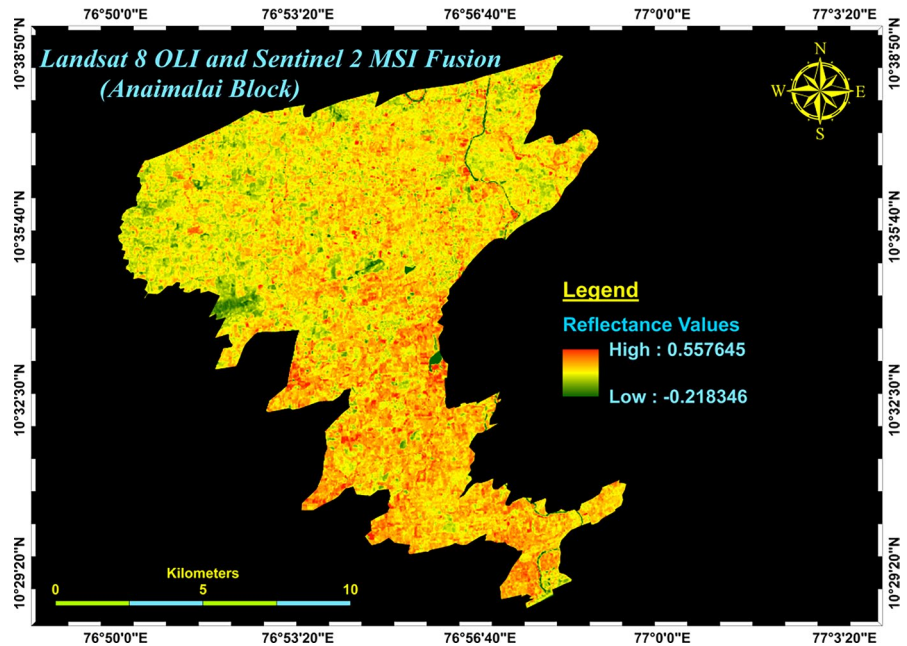


Fig. 3 a ATPRK 1 10-m downscaled Sentinel 2 data (Band 8A), b ATPRK 2 10-m downscaled Landsat 8 OLI data (Band 5), c layer-stacked 10-m downscaled Band 8A and Band 8 of Sentinel 2

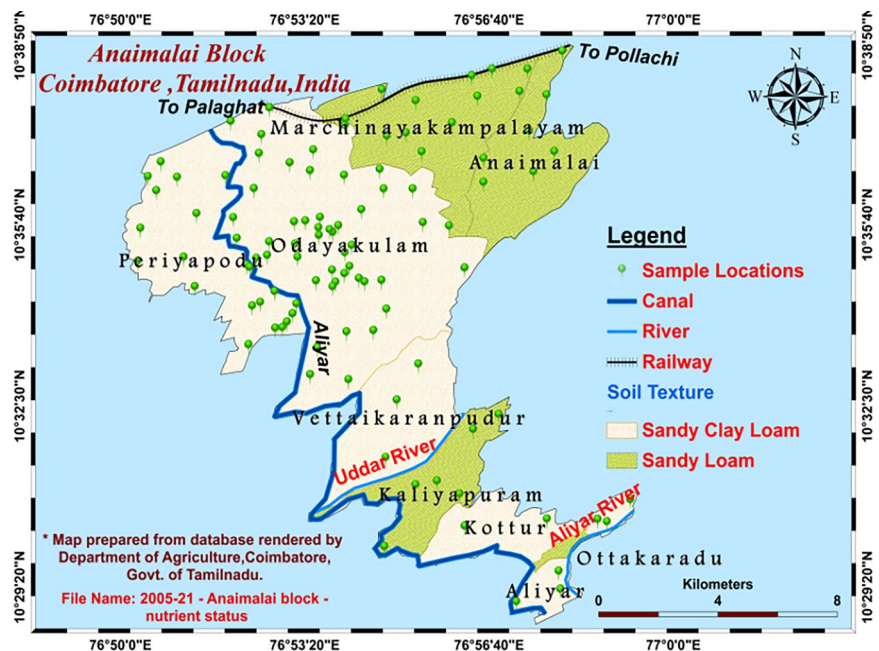
Fig. 4 ATPRK result produced by fusing the 10-m downscaled Landsat 8 OLI data (Band 5) with 10-m Sentinel 2 data (layer-stacked Band 8 and downscaled Band 8A)



white spectra were taken followed by the soil spectra for the samples were extracted (Fig. 6c). For the further analysis of extracted soil spectra, the data files are imported from spectroradiometer instruments to computer. In ViewSpec Pro software, the spectra were processed to convert the radiance files to desired reflectance files. The soil spectra is viewed

in the ENVI 4.7 software and the plot parameters is fixed from 400 to 1075 nm since the pre wavelength spectra were subjected to noise errors. The spectra are saved as ASCII files and the same has been opened in OrginPro 8.5 for further analysis of the soil spectra. From the datasets, only the reflectance values ranged from 700 to 900 nm (NIR Region) that can

Fig. 5 Sample locations and site description



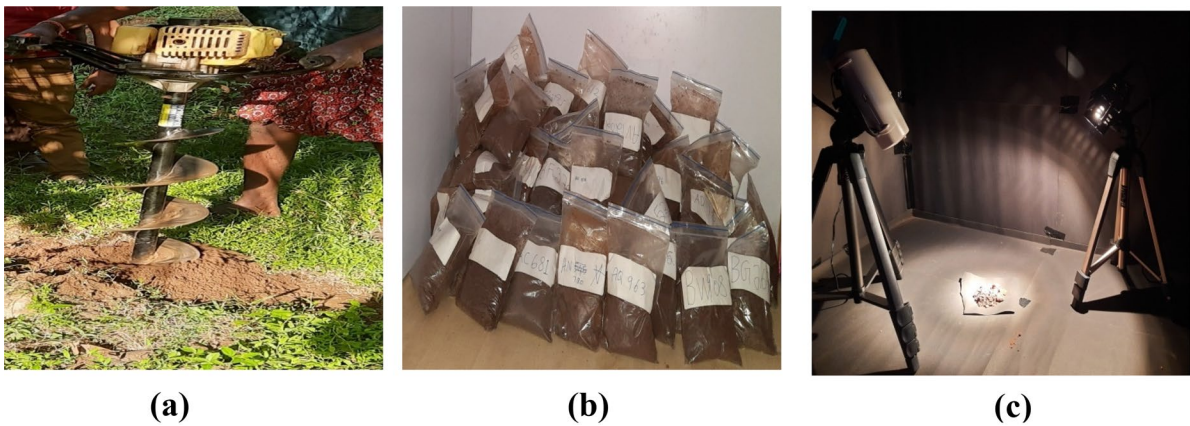


Fig. 6 a Soil sampling by using auger, b soil sample labeling, c in situ soil spectral extraction

match with the satellite dataset reflectance value were clipped. By importing the GCP points of 106 sample locations in the satellite data products (Landsat 8 OLI (Band 5), Sentinel 2 MSI (Band 8) and fused data product), the reflectance values were extracted in ArcGIS software. Now the reflectance values for 106 sample points in Landsat 8 OLI (Band 5), Sentinel 2 MSI (Band 8), and fused data product were compared with the in situ soil reflectance values.

Results and discussion

Regression analysis on in situ and Landsat 8 OLI

Fine values of reflectance extracted from Landsat 8 OLI (Band 5), Sentinel 2 MSI (Band 8), and fused data product were subjected to simple linear regression in OriginPro software. Linear regression-1 (LR-1) modeling was initiated for the reflectance values of Landsat 8 OLI (Band 5) that ranges from 845- to 885-nm wavelength and the reflectance values of soil in situ spectra. LR-1 reveals the correlation among both the reflectance values and possesses the R^2 value of 0.8209 and has the intercept of 0.1959 (Fig. 7a). Linear regression-2 (LR-2) modeling were initiated for the reflectance values of Sentinel 2 MSI (Band 8) that ranges from 785- to 900-nm wavelength and the reflectance values of soil in situ spectra. LR-2 reveals the association among the reflectance where the R^2 is found to be 0.843 and the intercept value of 0.154 (Fig. 7b). Linear

regression-3 (LR-3) modeling was initiated for the reflectance values of ATPRK-fused data product and the reflectance values of soil in situ spectra. LR-3 outcomes read the fine correlation among the reflectance with the R^2 value of 0.8763 and the intercept value of 0.154 (Fig. 7c). From the R^2 value, it is determined that the fused satellite product by using ATPRK technique finds the fine correlation than individual dataset.

Soil macronutrients assessment

The outcome of the regression analysis revealed the uniqueness of ATPRK approach fusion of Landsat 8 OLI and Sentinel 2 MSI through the predominant R^2 value comparable to a single-band soil characterization (Table 2). From the LR-3 model, it is inferred that reflectance of fused product finds close association with the soil properties. Although the soil reflectance consists of numerous properties and other phenomenon, the soil macronutrient status can be accessed through assigning the 106 sample NPK level to the corresponding soil reflectance values. Soil reflectance changes with change in the soil-measured nutrient values. Linear model was developed between the soil NPK measured value and fused reflectance value (Fig. 8) in order to delineate the equation for nitrogen, phosphorus, and potassium (Table 3). The linear regression equation follows the general equation theory as follows:

$$y = mx + c \tag{9}$$

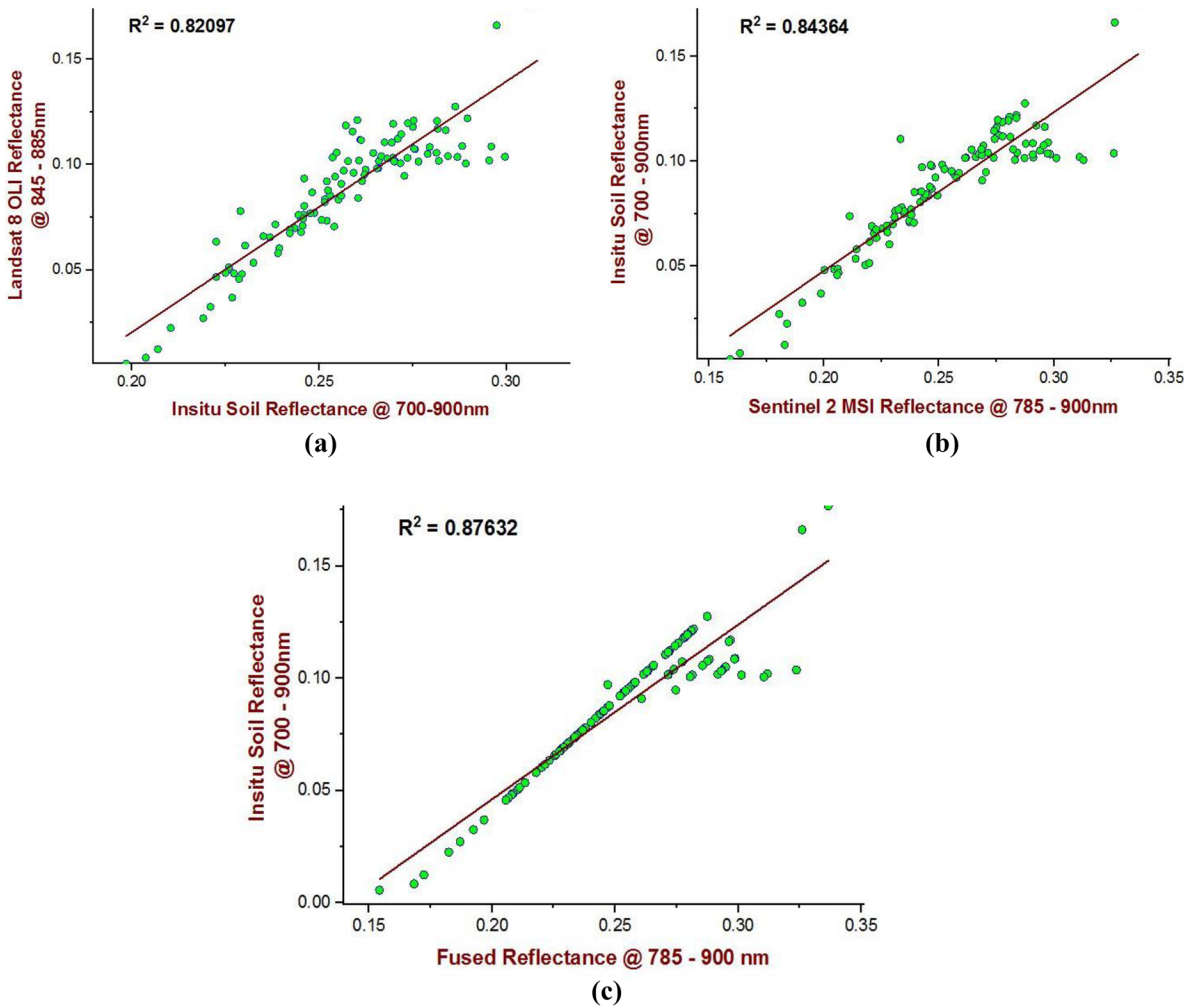


Fig. 7 Linear regression analysis (a), Landsat and in situ soil spectra (b), Sentinel 2 and in situ soil spectra (c), ATPRK-fused product and in situ soil spectra

where y =reflectance values corresponding to the nutrient value.

m =slope; c =intercept; x =dependent variable (in this study, x represents the soil nutrients).

Derived regression equation rendered as input to the fused data product and based on the reflectance value the corresponding NPK values are interpolated for each and every pixel this is based on the assigned NPK values to the reflectance. The assigned values for 106 sample location pixel will be the training dataset and based on the train sets the remaining pixels were interpolated with its corresponding equation. The corresponding equation x value will be unknown and the y value will be the reflectance

of the pixel.If the value of y is the reflectance of the pixel then the x value (nitrogen) can be calculated by $x = y - (0.25006 \pm 0.00754)/0.0000313$. Based on

Table 2 Regression model comparison

| Regression model | Parameters | R ² Value |
|------------------|----------------------------------------------|----------------------|
| LR-1 | Landsat and in situ soil spectra | 0.8209 |
| LR-2 | Sentinel 2 and in situ soil spectra | 0.8436 |
| LR-3 | ATPRK fused product and in situ soil spectra | 0.8763 |

LR linear regression

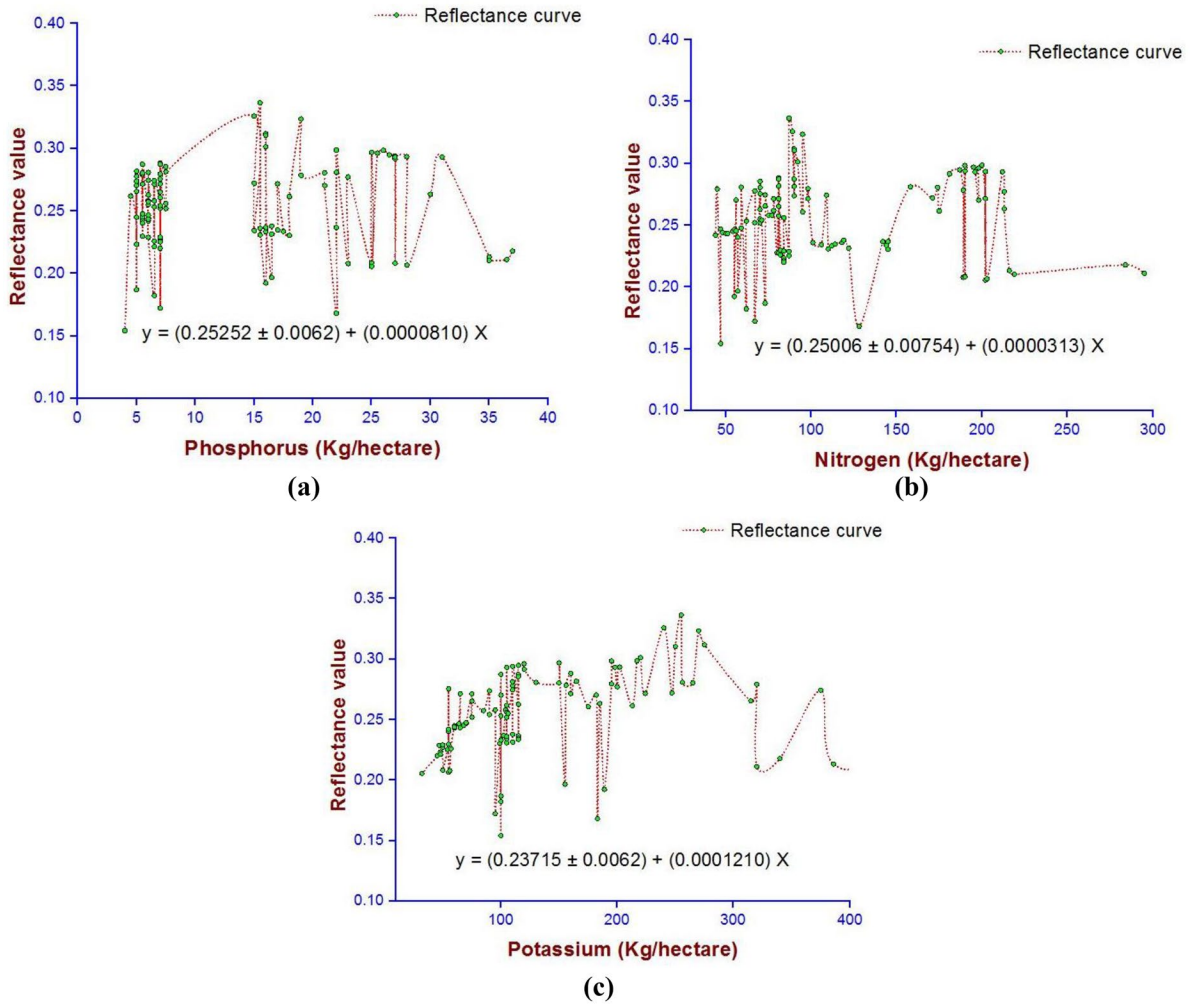


Fig. 8 Linear Regression model for **a** nitrogen, **b** phosphorus, **c** potassium

the corresponding equation for nitrogen, phosphorus, and potassium, the pixel-based values can be estimated. This has been estimated in ArcGIS software since GIS-based interpolation models support the decision analysis for agricultural productivity (Ozsahin & Ozdes, 2022). The estimated soil NPK level is mapped and reclassified according to the soil standards (Fig. 9).

Table 3 Linear regression model equation for soil NPK

| Soil macronutrients | Regression model equation |
|---------------------|--------------------------------------------|
| Nitrogen (N) | $y = (0.25006 \pm 0.00754) + (0.0000313)x$ |
| Phosphorus (P) | $y = (0.25252 \pm 0.0062) + (0.0000810)x$ |
| Potassium (K) | $y = (0.23715 \pm 0.0062) + (0.0001210)x$ |

Discussion

Remote sensing data products find numerous applications in the field of agriculture. Many data products have been utilized for close monitoring of day to day agricultural practices. In spite of all beneficial applications offered by satellite data product, there is an undiscovered ideology in the theme of periodical- and large-scale soil nutrient status. Precise soil nutrient database plays a vital role to attain the sustainable agriculture through suitable crop rotation at appropriate time with respect to soil nutrient and ecosystem. This paper contributes the ATPRK approaches in assessment of soil macronutrients in continuous monitoring. Numerous studies based on soil characteristics and nutrients

have been made. ATPRK fusion techniques were usually derived to categorize the land use and land cover changes (Chen et al., 2021). This study reveals the fact that the ATPRK fusion technique also preserves

the spectral information and moreover strengthens the spectral information. Downscaling of Landsat 8 OLI data product to match the spatial resolution of Sentinel 2 MSI data product preserves the spectral information

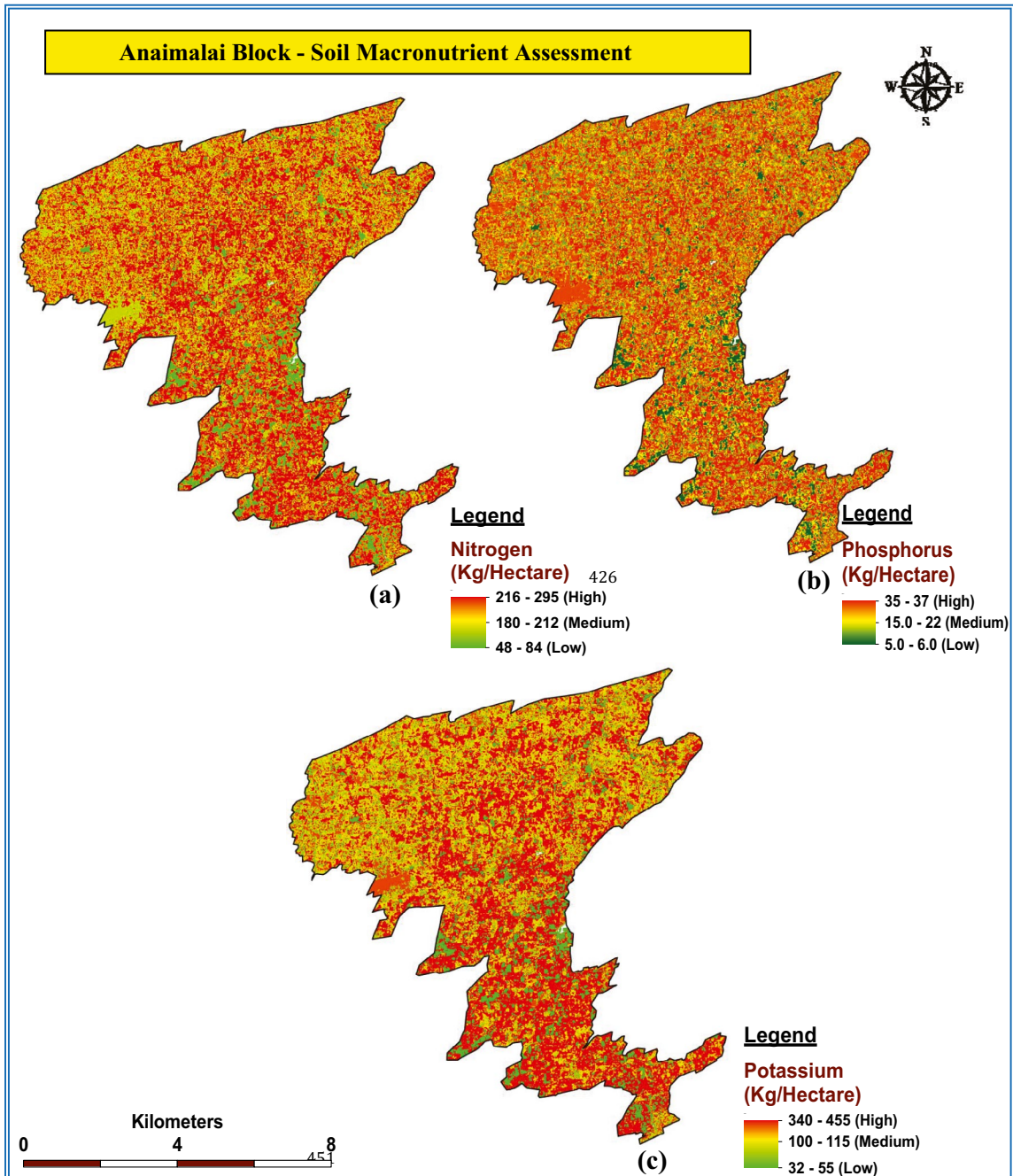


Fig. 9 Soil Assessment for Anaimalai block: **a** nitrogen, **b** phosphorus, **c** potassium

which was revealed from the R^2 value. Although the Sentinel data product has fine spectral information than the Landsat data product, some spectral information may be distorted due to various environmental factors such as cloud cover, missing spectral information, wrong reflectance value, and distorted pixels in Sentinel 2 data product (Demelash Beyene, 2021). In that occasion, the soil information on the distorted region of study may not be able to reveal or may give wrong direction of study (Stokes, 1996). Hence, it is recommended to utilize the fused satellite data product to obtain maximum information for precise decision making. The fusion technique by ATPRK finds solution to the aforementioned phenomenon. Shao et al. (2019) revealed that fusion of Landsat and Sentinel by ATPRK technique to study changes (LULC) and has achieved least RMSE value of 0.0178. The spatial information is concerned in LULC studies; whereas in soil health study, spectral information is much needed which is revealed in this study. Lin et al. (2020) represented soil organic matter based on Sentinel 2 and Sentinel 3 fusions by Gram-Schmidt method and obtained R^2 value of 0.6295 which is relatively lower than the ATPRK approach employed in this study ($R^2=0.8763$). Rajah et al. (2018) fused Landsat 8 and Sentinel 2 dataset by simple composite tools and derived multi seasonal distribution of plant species by correlating with ground truth variables. Techniques adopted are support vector algorithm to delineate the spectra resulted in 72–76% of accuracy which was comparatively lesser than the ATPRK approach which is carried out in this study (87% of accuracy). Close correlation with ATPRK result was observed with the study carried out by Li et al. in (2021), where MODIS and Landsat dataset were fused to interpolate crop species distribution by spatial and temporal adaptive reflectance fusion model. The derived R^2 value in that study found to be 0.70 fewer than this study. Moreover, MODIS dataset produce 92% of accuracy when compared to Sentinel 2 which can retrieve 94.8–96.8% of accuracy (Song et al., 2021). Thus, fusion of Landsat and Sentinel data product by ATPRK approaches give rise to soil nutrient interpolation than individual satellite product utility. As discussed in the review study, Odebiri et al. (2021) found that mapping soil nutrients information by utilizing multispectral datasets presents the soil properties at larger spatial extent. Incorporating this ideology in this study, the fused multispectral datasets were subjected to mapping based on the linear

regression model rendered by GIS tool. Komolafe et al. (2021) mapped soil nitrogen, phosphorus, and potassium by multiple linear regression models with the topographic features instead of fused spectral inputs which were incorporated in this study. Miran et al. (2021) found that linear regression model derived from Landsat OLI imagery could interpolate soil nitrogen better than phosphorus and potassium. The model derived for nitrogen, phosphorus, and potassium ($TN=0.9132 \times ZPC1 + 7.08R^2$, $P=-0.0144 \times ZPC1 + 0.13R^2$, and $K=-67.67 \times ZPC1 + 439.5R^2$ respectively) purely depends upon the principal component analysis of respective soil macronutrients; whereas in this study, the linear regression model for soil nitrogen, phosphorus, and potassium ($y=(0.25006 \pm 0.00754) + (0.0000313)x$, $y=(0.25252 \pm 0.0062) + (0.0000810)x$ and $y=(0.23715 \pm 0.0062) + (0.0001210)x$ respectively) depends upon soil-fused spectral reflectance value and laboratory-derived soil nutrients value. Comparatively, this study enhances the interpolation since two parameters were incorporated for rendering the model. In order to achieve the twenty-first century challenges such as managing and conserving soil resource without any deterioration for future generations, there is a great need for measuring the nutrient status inch by inch of the farm lands so as to follow multiple cropping protocols (Shrivastava et al., 2021). Multiple cropping is the only solution to resolve the food security problems, which is a major challenge in future as forecasted by the experts. Periodical inch by inch farm nutrient status for a large scale is feasible only through fusion of satellite data products. Time-series information about the soil health cannot be obtained by single satellite data product because of its slighter revisit time. Moreover, the single satellite product utilization at particular region of study is not possible at all the time although the revisit period of single satellite product is a regular one. Especially soil, sensitive parameters need more precise information to decide. The fertilization recommendation, crop cultivation, irrigation system, and other policy making in correspondence to soil health information can be decided through fused satellite data products information.

Conclusion

The obtained model equation can be given as input for every scenes of fused satellite product and consistent soil health can be monitored. From the results,

it is observed that the fusion technique enhances the soil health information and gives precise data rather than using individual satellite data products. Moreover, the current soil health status reveals that the land can be utilized for multicropping due to the availability of huge NPK level. Extensive literature reveals the particular utilization of band on a single-satellite data products. Fusing two or more data products enhance the information. Specifically, this study discusses the unique feature of ATPRK fusion of Landsat 8 OLI and Sentinel 2 MSI dataset that enhances the precise interpolation of soil macronutrients at the maximum extent. The assessed soil nutrient status reveals that the nitrogen, phosphorus, and potassium found high at the range of 216–295 kg/Hectare, 35–37 kg/Hectare, and 340–455 kg/Hectare respectively. Where only few regions suffer from low nutrient status more specifically, there is potassium deficiency in many of the agriculture fields that ranges from 32 to 55 kg/Hectare. Thus, this study fulfills the void research gaps in respect to time-series nutrient measurements and large scale compilation of soil nutrient status through area-to-point regression Kriging approach fusion of Landsat 8 OLI and Sentinel 2 data.

Acknowledgements We the authors grateful to support in the form of fellowship and encouragement received from SRM Institute of Science and Technology, Kattankulathur. It is pleasure to extend the acknowledgment to Vickram Muthu Rathinasabari for their valuable field assistance.

Author contribution Dhayalan V: Literature review, experimental design, analyzed, and interpreted the data Karuppasamy Sudalaimuthu: statistical analysis with graphical outcomes, conceptualization, drafting, and supervision.

Declarations

Competing interests The authors declare no competing interests.

References

Adiri, Z., Lhissou, R., El Harti, A., Jellouli, A., & Chakouri, M. (2020). Recent advances in the use of public domain satellite imagery for mineral exploration: A review of Landsat-8 and Sentinel-2 applications. *Ore Geology Reviews*, *117*, 103332. <https://doi.org/10.1016/j.oregeorev.2020.103332>

Armannsson, S. E., Ulfarsson, M. O., Sigurdsson, J., Nguyen, H. V., & Sveinsson, J. R. (2021). A comparison of optimized Sentinel-2 super-resolution methods using wald's

protocol and Bayesian optimization. *Remote Sensing*, *13*(11), 2192. <https://doi.org/10.3390/rs13112192>

Bolton, D. K., Gray, J. M., Melaas, E. K., Moon, M., Eklundh, L., & Friedl, M. A. (2020). Continental-scale land surface phenology from harmonized Landsat 8 and Sentinel-2 imagery. *Remote Sensing of Environment*, *240*, 111685. <https://doi.org/10.1016/j.rse.2020.111685>

Brede, B., Verrelst, J., Gastellu-Etchegorry, J. P., Clevers, J. G., Goudzwaard, L., Den Ouden, J., Verbesselt, J., & Herold, M. (2020). Assessment of workflow feature selection on forest LAI prediction with sentinel-2A MSI, landsat 7 ETM+ and Landsat 8 OLI. *Remote Sensing*, *12*(6), 915. <https://doi.org/10.3390/rs12060915>

Chen, B., Jing, L., & Yufang, J. (2021). Deep learning for feature-level data fusion: Higher resolution reconstruction of historical Landsat archive. *Remote Sensing*, *13*(2), 167. <https://doi.org/10.3390/rs13020167>

Dar, A., Zahir, Z. A., Iqbal, M., Mehmood, A., Javed, A., Hussain, A., & Ahmad, M. (2021). Efficacy of rhizobacterial exopolysaccharides in improving plant growth, physiology, and soil properties. *Environmental Monitoring and Assessment*, *193*(8), 1–15. <https://doi.org/10.1007/s10661-021-09286-6>

Demelash Beyene, M. (2021). *Crop Field Classification using fusion approach of unmanned aerial vehicle (UAV) and Sentinel 2A satellite data: The case of Oda Dhawata Kebele Cluster farmland, Oromia Region, Ethiopia* (Doctoral dissertation, Addis Ababa University). <http://hdl.handle.net/123456789/3517>

ED Chaves, M., CA Picoli, M., & D. Sanches, I. (2020). Recent applications of Landsat 8/OLI and Sentinel-2/MSI for land use and land cover mapping: A systematic review. *Remote Sensing*, *12*(18), 3062. <https://doi.org/10.3390/rs12183062>

Elbasiouny, H., Elbehiry, F., El-Ramady, H., & Brevik, E. C. (2020). Phosphorus availability and potential environmental risk assessment in alkaline soils. *Agriculture*, *10*(5), 172. <https://doi.org/10.3390/agriculture10050172>

Guimarães, C. C. B., Demattê, J. A., de Azevedo, A. C., Dalmolin, R. S. D., ten Caten, A., Sayão, V. M., da Silva, R. C., Poppiel, R. R., de Sousa Mendes, W., Salazar, D. F. U., & e Souza, A. B. (2021). Soil weathering behavior assessed by combined spectral ranges: Insights into aggregate analysis. *Geoderma*, *402*, 115154. <https://doi.org/10.1016/j.geoderma.2021.115154>

Gujre, N., Agnihotri, R., Rangan, L., Sharma, M. P., & Mitra, S. (2021). Deciphering the dynamics of glomalin and heavy metals in soils contaminated with hazardous municipal solid wastes. *Journal of Hazardous Materials*, *416*, 125869. <https://doi.org/10.1016/j.jhazmat.2021.125869>

Jagadala, K., & Sahoo, J. P. (2020). Critical limit of boron in acid laterite soil for cultivation of sunflower (*Helianthus annuus* L.). *IJCS*, *8*(3), 2510–2513. <https://doi.org/10.22271/chemi.2020.v8.i3aj.9588>

Jewan, S. Y. Y., Pagay, V., Billa, L., Tyerman, S. D., Gautam, D., Sparkes, D., Gautam, D., Sparkes, D., Chai, H.H., & Singh, A. (2021). The feasibility of using a low-cost near-infrared, sensitive, consumer-grade digital camera mounted on a commercial UAV to assess Bambara groundnut yield. *International Journal of Remote Sensing*, 1–31. <https://doi.org/10.1080/01431161.2021.1974116>

Kaman, S., & Makandar, A. (2021). Remote sensing of satellite images using digital image processing techniques:

A survey. *International Research Journal of Modernization in Engineering Technology and Science*, 3(1). Retrieved July 7, 2021, from https://www.irjmets.com/uploadedfiles/paper/volume_3/issue_7_july_2021/15221/final/fin_irjmets1632817612.pdf

Komolafe, A. A., Olorunfemi, I. E., Oloruntoba, C., & Akinluyi, F. O. (2021). Spatial prediction of soil nutrients from soil, topography and environmental attributes in the northern part of Ekiti State, Nigeria. *Remote Sensing Applications: Society and Environment*, 21, 100450. <https://doi.org/10.1016/j.rsase.2020.100450>

Leno, N., Sudharmaidevi, C. R., Byju, G., Thampatti, K. C. M., Krishnaprasad, P. U., Jacob, G., & Gopinath, P. P. (2021). Thermochemical digestate fertilizer from solid waste: Characterization, labile carbon dynamics, dehydrogenase activity, water holding capacity and biomass allocation in banana. *Waste Management*, 123, 1–14. <https://doi.org/10.1016/j.wasman.2021.01.002>

Li, R., Xu, M., Chen, Z., Gao, B., Cai, J., Shen, F., He, X., Zhuang, Y., & Chen, D. (2021). Phenology-based classification of crop species and rotation types using fused MODIS and Landsat data: The comparison of a random-forest-based model and a decision-rule-based model. *Soil and Tillage Research*, 206, 104838. <https://doi.org/10.1016/j.still.2020.104838>

Lin, C., Zhu, A. X., Wang, Z., Wang, X., & Ma, R. (2020). The refined spatiotemporal representation of soil organic matter based on remote images fusion of Sentinel-2 and Sentinel-3. *International Journal of Applied Earth Observation and Geoinformation*, 89, 102094. <https://doi.org/10.1016/j.jag.2020.102094>

Liu, X., & Wang, M. (2020). Super-resolution of VIIRS-measured ocean color products using deep convolutional neural network. *IEEE Transactions on Geoscience and Remote Sensing*, 59(1), 114–127. <https://doi.org/10.1109/TGRS.2020.2992912>

Miran, N., Rasouli Sadaghiani, M. H., Feiziasl, V., Sepehr, E., Rahmati, M., & Mirzaee, S. (2021). Predicting soil nutrient contents using Landsat OLI satellite images in rain-fed agricultural lands, northwest of Iran. *Environmental Monitoring and Assessment*, 193(9), 1–12. <https://doi.org/10.1007/s10661-021-09397-0>

Moravec, D., Komárek, J., López-Cuervo Medina, S., & Molina, I. (2021). Effect of atmospheric corrections on NDVI: Inter-comparability of Landsat 8, Sentinel-2, and UAV sensors. *Remote Sensing*, 13(18), 3550. <https://doi.org/10.3390/rs13183550>

Odebiri, O., Mutanga, O., Odindi, J., Naicker, R., Masemola, C., & Sibanda, M. (2021). Deep learning approaches in remote sensing of soil organic carbon: A review of utility, challenges, and prospects. *Environmental Monitoring and Assessment*, 193(12), 1–18. <https://doi.org/10.1007/s10661-021-09561-6>

Ozsahin, E., & Ozdes, M. (2022). Agricultural land suitability assessment for agricultural productivity based on GIS modeling and multi-criteria decision analysis: The case of Tekirdağ province. *Environmental Monitoring and Assessment*, 194(41), 1–19. <https://doi.org/10.1007/s10661-021-09663-1>

Papenfus, M., Schaeffer, B., Pollard, A. I., & Loftin, K. (2020). Exploring the potential value of satellite remote sensing to monitor chlorophyll-a for US lakes and reservoirs. *Environmental Monitoring and Assessment*, 192(12), 1–22. <https://doi.org/10.1007/s10661-020-08631-5>

Prada, M., Cabo, C., Hernández-Clemente, R., Hornero, A., Majada, J., & Martínez-Alonso, C. (2020). Assessing canopy responses to thinnings for sweet chestnut coppice with time-series vegetation indices derived from landsat-8 and sentinel-2 imagery. *Remote Sensing*, 12(18), 3068. <https://doi.org/10.3390/rs12183068>

Priem, F., Jilge, M., Heiden, U., Somers, B., & Canters, F. (2021, March). Towards a generic spectral library for urban mapping applications. In *EARSeL Joint Workshop 2021 Liège* (pp. 53–54). EARSeL. https://cris.vub.be/ws/portalfiles/portal/70696865/Abstract_Book_EarseL_Liege_2021.pdf

Rajah, P., Odindi, J., & Mutanga, O. (2018). Feature level image fusion of optical imagery and synthetic aperture radar (SAR) for invasive alien plant species detection and mapping. *Remote Sensing Applications: Society and Environment*, 10, 198–208. <https://doi.org/10.1016/j.rsase.2018.04.007>

Rathore, V. S., Nathawat, M. S., & Ray, P. C. (2008). Influence of neotectonic activity on groundwater salinity and playa development in the Mendha river catchment, western India. *International Journal of Remote Sensing*, 29(13), 3975–3986. <https://doi.org/10.1080/01431160801891861>

Scheffler, D., Frantz, D., & Segl, K. (2020). Spectral harmonization and red edge prediction of Landsat-8 to Sentinel-2 using land cover optimized multivariate regressors. *Remote Sensing of Environment*, 241, 111723. <https://doi.org/10.1016/j.rse.2020.111723>

Shen, H., Meng, X., & Zhang, L. (2016). An integrated framework for the spatio-temporal-spectral fusion of remote sensing images. *IEEE Transactions on Geoscience and Remote Sensing*, 54(12), 7135–7148. <https://doi.org/10.1109/TGRS.2016.2596290>

Shao, Z., Cai, J., Fu, P., Hu, L., & Liu, T. (2019). Deep learning-based fusion of Landsat-8 and Sentinel-2 images for a harmonized surface reflectance product. *Remote Sensing of Environment*, 235, 111425. <https://doi.org/10.1016/j.rse.2019.111425>

Shrestha, B., Ahmad, S., & Stephen, H. (2021). Fusion of Sentinel-1 and Sentinel-2 data in mapping the impervious surfaces at city scale. *Environmental Monitoring and Assessment*, 193(9), 1–21. <https://doi.org/10.1007/s10661-021-09321-6>

Shrivastava, A., Nayak, C. K., Dilip, R., Samal, S. R., Rout, S., & Ashfaq, S. M. (2021). Automatic robotic system design and development for vertical hydroponic farming using IoT and big data analysis. *Materials Today: Proceedings*. <https://doi.org/10.1016/j.matpr.2021.07.294>

Song, X. P., Huang, W., Hansen, M. C., & Potapov, P. (2021). An evaluation of Landsat, Sentinel-2, Sentinel-1 and MODIS data for crop type mapping. *Science of Remote Sensing*, 3, 100018. <https://doi.org/10.1016/j.still.2020.104838>

Stokes, M. A. (1996). *An introduction to tree-ring dating*. University of Arizona Press.

Taddia, Y., Russo, P., Lovo, S., & Pellegrinelli, A. (2020). Multi-spectral UAV monitoring of submerged seaweed in shallow water. *Applied Geomatics*, 12(1), 19–34. <https://doi.org/10.1007/s12518-019-00270-x>

Wang, Q., Blackburn, G. A., Onojeghuo, A. O., Dash, J., Zhou, L., Zhang, Y., & Atkinson, P. M. (2017). Fusion of

- Landsat 8 OLI and Sentinel-2 MSI data. *IEEE Transactions on Geoscience and Remote Sensing*, 55(7), 3885–3899. <https://doi.org/10.1109/TGRS.2017.2683444>
- Wang, Q., Wang, L., Wei, C., Jin, Y., Li, Z., Tong, X., & Atkinson, P. M. (2021). Filling gaps in Landsat ETM+ SLC-off images with Sentinel-2 MSI images. *International Journal of Applied Earth Observation and Geoinformation*, 101, 102365. <https://doi.org/10.1016/j.jag.2021.102365>
- Wiyantoko, B., Maulidatunnisa, V., & Purbaningtias, T. E. (2021, September). Method performance of K2O analysis in flake potassium fertilizer using flame photometer. In *AIP Conference Proceedings* (Vol. 2370, No. 1, p. 030008). AIP Publishing LLC. <https://doi.org/10.1063/5.0062537>
- Xu, Y., Fan, H., & Dang, L. (2021). Monitoring coal seam fires in Xinjiang using comprehensive thermal infrared and time series InSAR detection. *International Journal of Remote Sensing*, 42(6), 2220–2245. <https://doi.org/10.1080/01431161.2020.1823045>
- Zhang, Y., Ling, F., Wang, X., Foody, G. M., Boyd, D. S., Li, X., Du, Y., & Atkinson, P. M. (2021). Tracking small-scale tropical forest disturbances: Fusing the Landsat and Sentinel-2 data record. *Remote Sensing of Environment*, 261, 112470. <https://doi.org/10.1016/j.rse.2021.112470>
- Zheng, H., Zhou, X., He, J., Yao, X., Cheng, T., Zhu, Y., Cao, W., & Tian, Y. (2020). Early season detection of rice plants using RGB, NIR-GB and multispectral images from unmanned aerial vehicle (UAV). *Computers and Electronics in Agriculture*, 169, 105223. <https://doi.org/10.1016/j.compag.2020.105223>
- Zhou, J., Qiu, Y., Chen, J., & Chen, X. (2021). A geometric misregistration resistant data fusion approach for adding red-edge (RE) and short-wave infrared (SWIR) bands to high spatial resolution imagery. *Science of Remote Sensing*, 100033. <https://doi.org/10.1016/j.srs.2021.100033>

Publisher's Note Springer Nature remains neutral with regard to jurisdictional claims in published maps and institutional affiliations.

Springer Nature or its licensor holds exclusive rights to this article under a publishing agreement with the author(s) or other rightsholder(s); author self-archiving of the accepted manuscript version of this article is solely governed by the terms of such publishing agreement and applicable law.